Free-surface thin-film flows over uniformly heated topography

Sergey Saprykin,[1] Philip M. J. Trevelyan,[1] Rudy J. Koopmans,[2] and Serafim Kalliadasis[1]
[1]*Department of Chemical Engineering, Imperial College London, London SW7 2AZ, United Kingdom*
[2]*Core R&D, Dow Benelux B.V., 4530 AA Terneuzen, The Netherlands*

(Received 10 April 2006; revised manuscript received 6 October 2006; published 8 February 2007)

The long-wave (lubrication) approximation governing the evolution of a thin film over a uniformly heated topographical substrate is solved numerically. We study the initial-value problem for a variety of governing dimensionless parameters and topographical substrates. We demonstrate that the dynamics is characterized by a slow relaxation process with continuous coarsening of drops up to a large time where coarsening is terminated and the interface organizes into a series of drops each of which is located in a trough in topography.

DOI: 10.1103/PhysRevE.75.026306 PACS number(s): 47.15.gm, 47.55.nb, 47.55.nd, 68.03.Kn

I. INTRODUCTION

The response of thin liquid films to external forcing is a well-studied area. The forcing could be due to thermocapillary Marangoni stresses—i.e., stresses due to variation of surface tension along a liquid interface induced by temperature gradients along the liquid layer. Several studies have been devoted to the dynamics of a falling liquid film with a substrate heated either uniformly [1–8] or by a local heat source [9–11], the dynamics of a falling liquid film in the presence of exothermic chemical reactions taking place in the film [12–14], and the evolution of an horizontal thin liquid film heated uniformly from below [15–24]. The forcing could also be topographical. Free-surface thin-film flows over topography are also a well-studied area [25–30].

In this study we examine the dynamics of a thin liquid film in the presence of a uniformly heated topography and hence in the presence of both forcing factors. The aim is to analyze the interaction of the two effects. Two-dimensional (2D) (1+1 dimensions) flows over uniformly heated substrates were recently analyzed by Alexeev *et al.* [31] who solved numerically the full 2D Navier-Stokes equations for flow over a regular topography, either sinusoidal or a series of grooves, and by Kabova *et al.* [32] who demonstrated for the same problem that a 2D long-wave (lubrication) model is in good agreement with the full 2D Navier-Stokes equations. However, in these studies the computations were stopped when the minimum film thickness reached a very small value. At this point film rupture occurs followed by the formation of dry patches. In the present study, instead of rupture and completely dry domains, the solid substrate is always covered by a thin precursor film. This is accomplished through a disjoining pressure model that depends on a single intermolecular force parameter and prevents the film from breaking. This allows us to scrutinize the coupling between topography and Marangoni effect and determine the long-time evolution of a film which is unstable due to the Marangoni effect induced by the heated topographical substrate. We consider both 2D and 3D (2+1 dimensions) flows and a variety of topographical substrates, both regular and irregular. Our starting point is the 3D long-wave (lubrication) approximation that includes the disjoining pressure as an extra body force. The approximation leads to a single nonlinear partial differential equation for the evolution of the local film thickness in time and space. Fully nonlinear time-dependent computations reveal that for large times the interface organizes into a series of drops each of which is situated in the troughs of the topography. Hence, free-surface flows over uniformly heated topographical substrates behave differently from those over uniformly heated flat substrates where the final result of the evolution is a single drop (or hole) [21]. Finally, we examine chemically heterogeneous topographical substrates and investigate the possibility of minimizing the drops forming into the troughs of the topography by locally varying the intermolecular parameter.

II. FORMULATION

A. Governing equations

We consider a thin liquid film on a uniformly heated topographical substrate. Figure 1 sketches the flow situation. The heating is provided by a heat source inside the substrate that uniformly generates heat—e.g., an electric heating device. For simplicity we shall employ approximate boundary conditions at the liquid-gas and liquid-wall interfaces, thus bypassing the much more involved conjugated heat transfer problems in the air and the wall: on the free surface we assume Newton's law of cooling while on the wall the heater is assumed to maintain the wall temperature at a constant value T_w. The heating provided by the wall induces a thermocapillary Marangoni effect which affects the evolution of the interface and therefore the fluid flow.

The liquid film has viscosity μ, density ρ, kinematic viscosity $\nu=\mu/\rho$, constant pressure heat capacity c_p, thermal diffusivity κ, and thermal conductivity $\lambda=\rho c_p \kappa$, all assumed to be constant. We also assume that the liquid is nonvolatile so that evaporation effects can be neglected while the film is sufficiently thin so that buoyancy effects can be neglected. The governing equations are continuity, Navier-Stokes, and energy:

$$\nabla \cdot \mathbf{v} = 0, \tag{1a}$$

$$\rho(\partial_t + \mathbf{v}\cdot\nabla)\mathbf{v} = -\nabla p + \mu\nabla^2\mathbf{v} + \rho\mathbf{g}, \tag{1b}$$

$$(\partial_t + \mathbf{v}\cdot\nabla)T = \kappa\nabla^2 T, \tag{1c}$$

where $\nabla=(\partial_x,\partial_y,\partial_z)$ is the gradient operator, $\mathbf{v}=(u,v,w)$, p, and T are the velocity vector, pressure, and temperature of

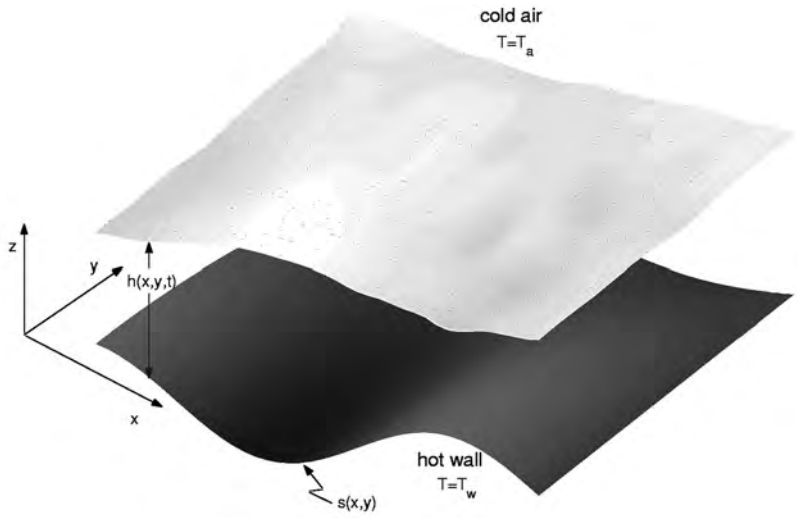

FIG. 1. Flow over heated topography with shape $s(x,y)$ with respect to a datum plane $z=0$. The relative film thickness is $h(x,y,t)$. The topography is maintained at the constant temperature T_w. The surrounding gas phase is air maintained at the constant temperature T_a ($<T_w$).

the liquid, respectively, and $\mathbf{g}=(0,0,-g)$ is the body force.

These equations are subject to the following boundary conditions. On the wall we have the usual no-slip boundary condition

$$\mathbf{v}=\mathbf{0} \quad \text{on} \quad z=s(x,y) \tag{2a}$$

and the specified wall temperature

$$T=T_w \quad \text{on} \quad z=s(x,y). \tag{2b}$$

On the interface $z=H(x,y,t)\equiv h(x,y,t)+s(x,y)$ we have the kinematic boundary condition along with the normal and tangential stress balances:

$$\partial_t h+\mathbf{v}\cdot\boldsymbol{\nabla}H=w, \quad p_a+(\boldsymbol{\tau}\cdot\mathbf{n})\cdot\mathbf{n}+\Pi=2\sigma K(H),$$

$$(\boldsymbol{\tau}\cdot\mathbf{n})\cdot\mathbf{t}_i=\boldsymbol{\nabla}_s\sigma\cdot\mathbf{t}_i; \quad i=1,2, \tag{2c}$$

where $\mathbf{n}$ and $\mathbf{t}_i$ are unit vectors, normal (outward pointing) and tangential to the interface, respectively, defined from $\mathbf{n}=n^{-1}(-\partial_x H,-\partial_y H,1)$, $\mathbf{t}_1=t_1^{-1}(1,0,\partial_x H)$, $\mathbf{t}_2=t_2^{-1}(0,1,\partial_y H)$, where $n=[1+(\partial_x H)^2+(\partial_y H)^2]^{1/2}$, $t_1=[1+(\partial_x H)^2]^{1/2}$, and $t_2=[1+(\partial_y H)^2]^{1/2}$. $K(H)=-(1/2)\boldsymbol{\nabla}\cdot\mathbf{n}$ is the curvature of the interface, and $\boldsymbol{\nabla}_s$ is the surface gradient operator originating from the decomposition of the gradient operator $\boldsymbol{\nabla}$ on the film surface as $\boldsymbol{\nabla}=(\mathbf{I}-\mathbf{nn})\cdot\boldsymbol{\nabla}+\mathbf{nn}\cdot\boldsymbol{\nabla}=\boldsymbol{\nabla}_s+\mathbf{nn}\cdot\boldsymbol{\nabla}$, where $\mathbf{I}$ the identity matrix and $\mathbf{nn}$ is the dyadic product of the normal vector $\mathbf{n}$ with itself. $\boldsymbol{\tau}=-p\mathbf{I}+2\mu\mathbf{e}$ is the stress tensor with $\mathbf{e}$ the rate-of-strain tensor given by $e_{ij}=(1/2)(\partial_{x_j}u_i+\partial_{x_i}u_j)$. p_a is the pressure of the ambient gas phase, σ is the surface tension, and Π is the disjoining pressure that expresses long-range van der Walls intermolecular interactions between the solid and gas phases separated by the liquid phase (these interactions are added in the normal stress balance as an extra distributed body force—effectively as an extra term in the liquid pressure). The thermal boundary condition on the free surface is

$$\lambda\,\boldsymbol{\nabla}T\cdot\mathbf{n}=-\alpha_g(T-T_a), \quad \text{on} \quad z=H(x,y,t), \tag{2d}$$

where α_g is the heat transfer coefficient describing the rate of heat transport from the liquid to the ambient gas phase. Finally, the thermocapillary Marangoni effect is modeled using a linear approximation for the surface tension:

$$\sigma=\sigma_a-\gamma(T-T_a), \tag{3}$$

where σ_a is the surface tension at the reference temperature T_a and $\gamma>0$ for typical liquids.

B. Scalings and nondimensionalization

We now introduce the nondimensionalization

$$(x,y)\to\ell(x,y), \quad (z,h,s)\to h_0(z,h,s),$$

$$(u,v)\to\epsilon u_0(u,v), \quad w\to\epsilon^2 u_0 w,$$

$$t\to\frac{\ell}{\epsilon u_0}t, \quad (p-p_a,\Pi)\to\rho g h_0(p,\Pi),$$

$$T\to T_a+(T_w-T_a)T,$$

where ℓ is a characteristic lengthscale of the topography, h_0 is the mean film thickness, $u_0=gh_0^2/\nu$, and $\epsilon=h_0/\ell$, the "film parameter." Temperature scales with T_w-T_a which would be the control variable in an actual experiment.

In terms of these nondimensional variables, the equations of motion, continuity, and energy in Eqs. (1) become

$$\partial_x u+\partial_y v+\partial_z w=0, \tag{4a}$$

$$\epsilon\,\mathrm{Re}(\partial_t u+u\partial_x u+v\partial_y u+w\partial_z u)=-\partial_x p+\epsilon^2\partial_{xx}u+\epsilon^2\partial_{yy}u+\partial_{zz}u, \tag{4b}$$

$$\epsilon\,\mathrm{Re}(\partial_t v+u\partial_x v+v\partial_y v+w\partial_z v)=-\partial_y p+\epsilon^2\partial_{xx}v+\epsilon^2\partial_{yy}v+\partial_{zz}v, \tag{4c}$$

$$\epsilon^3\,\mathrm{Re}(\partial_t w+u\partial_x w+v\partial_y w+w\partial_z w)=-\partial_z p+\epsilon^4\partial_{xx}w+\epsilon^4\partial_{yy}w+\epsilon^2\partial_{zz}w-1, \tag{4d}$$

$$\epsilon \,\mathrm{Re}\,\mathrm{Pr}(\partial_t T + u\partial_x T + v\partial_y T + w\partial_z T) = \epsilon^2\partial_{xx}T + \epsilon^2\partial_{yy}T + \partial_{zz}T, \tag{4e}$$

with $\mathrm{Re}=u_0h_0/\nu$ the Reynolds number and $\mathrm{Pr}=\nu/\kappa$ the Prandtl number. Note that the product Re Pr is the Péclet number for heat transport that measures the relative importance of conduction over convection. The wall boundary conditions in Eqs. (2a) and (2b) become

$$u = v = w = 0, \quad T = 1, \quad \text{on} \quad z = s(x,y), \tag{5a}$$

while the interfacial boundary conditions at $z=H(x,y,t)$, Eq. (2c), become

$$\partial_t h + u\partial_x H + v\partial_y H = w, \tag{5b}$$

$$\begin{aligned} p &- 2\epsilon^2 N^{-2}[\partial_z w - \partial_x H(\partial_z u + \epsilon^2\partial_x w) - \partial_y H(\partial_z v + \epsilon^2\partial_y w)] \\ &- 2\epsilon^4 N^{-2}[\partial_x H\partial_y H(\partial_y u + \partial_x v) + (\partial_x H)^2\partial_x u + (\partial_y H)^2\partial_y v] \\ &+ \epsilon^2\left(\frac{1}{\mathrm{Bo}} - \mathrm{Ma}T\right)N^{-3}(N_x^2\partial_{yy}H + N_y^2\partial_{xx}H \\ &- 2\epsilon^2\partial_x H\partial_y H\partial_{xy}H) + \Pi = 0, \end{aligned} \tag{5c}$$

$$\begin{aligned} [1 &- \epsilon^2(\partial_x H)^2](\partial_z u + \epsilon^2\partial_x w) + 2\epsilon^2\partial_x H(\partial_z w - \partial_x u) \\ &- \epsilon^2\partial_y H(\partial_y u + \partial_x v) - \epsilon^2\partial_x H\partial_y H(\partial_z v + \epsilon^2\partial_y w) \\ &= -\epsilon\mathrm{Ma}N(\partial_x T + \partial_x H\partial_z T), \end{aligned} \tag{5d}$$

$$\begin{aligned} [1 &- \epsilon^2(\partial_y H)^2](\partial_z v + \epsilon^2\partial_y w) + 2\epsilon^2\partial_y H(\partial_z w - \partial_y v) \\ &- \epsilon^2\partial_x H(\partial_y u + \partial_x v) - \epsilon^2\partial_x H\partial_y H(\partial_z u + \epsilon^2\partial_x w) \\ &= -\epsilon\mathrm{Ma}N(\partial_y T + \partial_y H\partial_z T), \end{aligned} \tag{5e}$$

$$(\partial_z T - \epsilon^2\partial_x T\partial_x H - \epsilon^2\partial_y T\partial_y H)N^{-1} = -\mathrm{Bi}T, \tag{5f}$$

where $N=[1+\epsilon^2(\partial_x H)^2+\epsilon^2(\partial_y H)^2]^{1/2}$, $N_x=[1+\epsilon^2(\partial_x H)^2]^{1/2}$, and $N_y=[1+\epsilon^2(\partial_y H)^2]^{1/2}$. $\mathrm{Ma}=\gamma(T_w-T_a)/(\mu u_0)$ is the Marangoni number that expresses the relative importance of thermocapillary over viscous stresses, $\mathrm{Bo}=\rho g h_0^2/\sigma_a$ is the static Bond number that expresses the relative importance of gravity over surface tension (it can be written in terms of the Weber number We as $\mathrm{Bo}=\mathrm{We}^{-1}$ [33]), and $\mathrm{Bi}=\alpha_g h_0/\lambda$ is the Biot number.

C. Long-wave approximation

The complexity of the free-boundary value problem in Eqs. (4) and (5) can be removed by invoking a long-wave (lubrication) approximation for $\epsilon \ll 1$. This allows an asymptotic reduction of the governing equations and boundary conditions to a single nonlinear partial differential equation of the evolution type formulated in terms of the local film thickness. A detailed review of long-wave theories for flat substrates is given in Ref. [34]. Note that the fundamental difference with flow over a flat substrate is that now the long-wave parameter is known *a priori*. In fact, the lubrication approximation could be based on two small parameters $\epsilon=h_0/\ell$ and $\epsilon'=D/\ell$, with D a characteristic amplitude of the topography; i.e., perform the long-wave expansion for both free surface and topography. Different relative orders will in general lead to different long-wave evolution equations. For example, $\epsilon \ll \epsilon' \ll 1$ would be the case of a "thin" film on a "large" topography. Here we consider the distinguished limit $\epsilon \sim \epsilon' \ll 1$ as is evident from the fact that both h and s scale with h_0.

For the disjoining pressure in Eq. (5c) we adopt a model introduced by Schwartz [35] (see also Schwartz *et al.* [36,37]) for flows over flat substrates in the form $\Pi = A[(h_*/h)^n-(h_*/h)^m] \equiv A\mathrm{P}(h)$ where A is a positive parameter that measures the strength of the disjoining pressure and the exponents n and m are positive constants with $n>m>1$. For such flows, this disjoining pressure avoids film rupture due to the Marangoni effect, which restricts the computations to small times. The first term represents liquid-solid repulsion, while the second term is attractive. Hence the first term prevents rupture while the second term leads to rupture. The balance of the two leads to a stable precursor layer of thickness h_*. Indeed, the local disjoining energy density $e(h)=-\int_{h_*}^{h}\Pi(h')dh'$ has a single stable energy minimum at the thin precursor-layer thickness $h=h_*$ [36,37]. We shall demonstrate that a stable precursor layer of thickness h_* exists also for flows over topography. Note that the above expression for the disjoining pressure is valid for nearly parallel interfaces as it depends on the local interfacial separation h only and hence the validity of this expression requires the long-wave approximation. Finally, in terms of the nondimensionalization introduced earlier, the disjoining pressure term in Eq. (5c) becomes $\Pi=B\mathrm{P}(h)$ where the dimensionless parameter B is defined as $B=A/(\rho g h_0)$.

Further we assume that Ma, Re, Pr, $B=O(1)$, Bi is at most $O(1)$, and $\mathrm{Bo}=O(\epsilon^2)$. We then obtain to leading order in ϵ from Eqs. (4) and (5),

$$\partial_x u + \partial_y v + \partial_z w = 0, \tag{6a}$$

$$\partial_x p = \partial_{zz} u, \tag{6b}$$

$$\partial_y p = \partial_{zz} v, \tag{6c}$$

$$\partial_z p = -1, \tag{6d}$$

$$\partial_{zz} T = 0, \tag{6e}$$

subject to the boundary conditions on $z=s(x,y)$,

$$u = v = w = 0, \quad T = 1, \tag{7a}$$

and on $z=H(x,y,t)$,

$$p = -\frac{\epsilon^2}{\mathrm{Bo}}\nabla^2 H - B\mathrm{P}(h), \tag{7b}$$

$$\partial_z u = -\mathrm{Ma}(\partial_x T + \partial_x H\partial_z T), \tag{7c}$$

$$\partial_z v = -\mathrm{Ma}(\partial_y T + \partial_y H\partial_z T), \tag{7d}$$

$$\partial_z T = -\mathrm{Bi}T, \tag{7e}$$

$$\partial_t h + u\partial_x H + v\partial_y H = w, \tag{7f}$$

where for convenience now $\boldsymbol{\nabla}=(\partial_x,\partial_y)$, the gradient operator on the (x,y) plane. Note that Eq. (7b) shows clearly the influence of the topography on the film: the capillary part of the pressure is a superposition of two contributions: the usual interfacial curvature term due to surface tension $\boldsymbol{\nabla}^2 h$ and the interfacial curvature $\boldsymbol{\nabla}^2 s$ created by the topography.

The solution of the above system (6) and (7) is facilitated by the introduction of a 3D stream function $\mathbf{v}=\boldsymbol{\nabla}\times\boldsymbol{\Psi}$ where $\boldsymbol{\Psi}=(\Phi,-\Psi,0)$ so that $u=\partial_z\Psi$, $v=\partial_z\Phi$, and $w=-\partial_x\Psi-\partial_y\Phi$ and the continuity equation (6a) is then automatically satisfied. The solution of the temperature equation (6e), which satisfies the temperature boundary conditions (7a) and (7e) is

$$T = 1 - \frac{\mathrm{Bi}(z-s)}{1+\mathrm{Bi}h}. \tag{8}$$

The solution of the pressure equation (6d), which satisfies the boundary condition (7b), is

$$p = -\frac{\epsilon^2}{\mathrm{Bo}}\boldsymbol{\nabla}^2 H - B\mathsf{P}(h) - z + H. \tag{9}$$

By utilizing now the stream function $\boldsymbol{\Psi}$, the pressure equations (6b) and (6c) are written as $\partial_x p=\partial_{zzz}\Psi$ and $\partial_y p=\partial_{zzz}\Phi$ which by using Eq. (9) can be integrated 3 times to give

$$\Psi = -\frac{1}{6}\left(\frac{\epsilon^2}{\mathrm{Bo}}\boldsymbol{\nabla}^2\partial_x H + B\partial_x\mathsf{P} - \partial_x H\right)(z-s)^3 + a_{11}(z-s)^2 + a_{12}(z-s) + a_{13}, \tag{10a}$$

$$\Phi = -\frac{1}{6}\left(\frac{\epsilon^2}{\mathrm{Bo}}\boldsymbol{\nabla}^2\partial_y H + B\partial_y\mathsf{P} - \partial_y H\right)(z-s)^3 + a_{21}(z-s)^2 + a_{22}(z-s) + a_{23}. \tag{10b}$$

We now turn to the no-slip boundary condition (7) which in terms of $\boldsymbol{\Psi}$ can be written as $\Psi=\Phi=\partial_z\Psi=\partial_z\Phi=0$ on $z=s$. We then obtain from (10a) and (10b) $a_{12}=a_{13}=a_{22}=a_{23}=0$. On the other hand, substituting the temperature field (8) into the Marangoni stress boundary conditions (7c) and (7d) expressed in terms of $\boldsymbol{\Psi}$ yields

$$\partial_{zz}\Psi = \frac{\mathrm{Ma\ Bi}\ \partial_x h}{(1+\mathrm{Bi}h)^2}, \quad \partial_{zz}\Phi = \frac{\mathrm{Ma\ Bi}\ \partial_y h}{(1+\mathrm{Bi}h)^2},$$

which combined with Eqs. (10a) and (10b) determine the remaining parameters:

$$a_{11} = \frac{1}{2}\left[\frac{\mathrm{Ma\ Bi}\ \partial_x h}{(1+\mathrm{Bi}h)^2} + h\left(\frac{\epsilon^2}{\mathrm{Bo}}\boldsymbol{\nabla}^2\partial_x H + B\partial_x\mathsf{P} - \partial_x H\right)\right],$$

$$a_{21} = \frac{1}{2}\left[\frac{\mathrm{Ma\ Bi}\ \partial_y h}{(1+\mathrm{Bi}h)^2} + h\left(\frac{\epsilon^2}{\mathrm{Bo}}\boldsymbol{\nabla}^2\partial_y H + B\partial_y\mathsf{P} - \partial_y H\right)\right].$$

We then have from Eqs. (10a) and (10b)

$$\Psi = (z-s)^2\left(\frac{\epsilon^2}{\mathrm{Bo}}\boldsymbol{\nabla}^2\partial_x H + B\partial_x\mathsf{P} - \partial_x H\right)\left(\frac{1}{2}h - \frac{1}{6}(z-s)\right) + \frac{\mathrm{Ma\ Bi}\ \partial_x h}{2(1+\mathrm{Bi}h)^2}(z-s)^2, \tag{10c}$$

$$\Phi = (z-s)^2\left(\frac{\epsilon^2}{\mathrm{Bo}}\boldsymbol{\nabla}^2\partial_y H + B\partial_y\mathsf{P} - \partial_y H\right)\left(\frac{1}{2}h - \frac{1}{6}(z-s)\right) + \frac{\mathrm{Ma\ Bi}\ \partial_y h}{2(1+\mathrm{Bi}h)^2}(z-s)^2. \tag{10d}$$

The free-surface evolution equation can then be obtained from the kinematic boundary condition (7f) which in terms of $\boldsymbol{\Psi}$ can be written as

$$\partial_t h + \partial_x(\Psi(H)) + \partial_y(\Phi(H)) = 0, \tag{11}$$

where $\Psi(H)$ and $\Phi(H)$ are given by Eqs. (10c) and (10d). It is convenient to introduce in this equation the reduced Bond number $\mathrm{Bo}'=\mathrm{Bo}/\epsilon^2$ $[=O(1)]$ and modified Marangoni number and intermolecular parameter $\mathrm{Ma}'=3\mathrm{Ma\ Bo}'$ and $B'=B\ \mathrm{Bo}'$, respectively, and to rescale the space coordinate as $t'=t/(3\mathrm{Bo}')$. After dropping the primes, the final evolution equation is

$$\partial_t h + \frac{1}{2}\mathrm{Ma\ Bi}\ \boldsymbol{\nabla}\cdot\left(\frac{h^2}{(1+\mathrm{Bi}h)^2}\boldsymbol{\nabla}h\right) - \mathrm{Bo}\ \boldsymbol{\nabla}\cdot(h^3\boldsymbol{\nabla}H) + \boldsymbol{\nabla}\cdot[h^3\boldsymbol{\nabla}(\boldsymbol{\nabla}^2 H + B\mathsf{P})] = 0. \tag{12}$$

The second term in this equation is due to the Marangoni effect, the third term is due to the hydrostatic head, and the last two terms are the curvature gradient associated with surface tension and the contribution of the intermolecular forces. Hence, the final evolution equation (12) has the Bond number in front of the hydrostatic force term unlike Eq. (11) where the Bond number multiplies the capillary force terms.

The system is governed by four dimensionless groups Ma, Bi, Bo, and B. Note that the Marangoni and Biot numbers appear Eq. (12) through their product only. As a consequence, the limits $\mathrm{Ma}\to 0$ and $\mathrm{Bi}\to 0$ both lead to the Marangoni term in Eq. (12) vanishing, even though the two parameters represent different and, in general, unrelated physical processes. Indeed, for an insulated interface and hence vanishing heat flux there, the temperature is everywhere uniform and equal to the wall temperature as is also evident from Eq. (8). As a result there is no Marangoni instability. As a matter of fact, the temperature equals the wall temperature at all orders in ϵ as can be easily seen by substituting the long-wave expansion $T\sim T^0+\epsilon T^1+\cdots$ into the energy equation (4) and solving for the higher-order terms [with T^0 given by Eq. (8)]. Hence, the temperature remains equal to the wall temperature for any deformation of the free surface.

III. VALUES OF DIMENSIONAL AND DIMENSIONLESS PARAMETERS

Typical values of the various dimensional parameters if the liquid phase is water at 25 °C are [38,39] $\mu=1$ cp, σ_a

$=60$ dyn/cm, $\rho=1$ g/cm^3, $\gamma=5\times10^{-5}$ N/(mK), and $\lambda=0.6$ W/(mK). If the liquid phase is one of the light solicone oils (polydimethylsiloxanes or PDMS) used frequently in wetting dynamics experiments such as silicone oil 50 cS at 25 °C (e.g., [21,40]; such oils have low interfacial tensions, they completely wet many types of substrates, and they are insensitive to substrate contamination), then $\mu=50$ cp, $\sigma_a=20$ dyn/cm, $\rho=0.96$ g/cm^3, $\gamma=6.8\times10^{-5}$ N/(mK), and $\lambda=0.15$ W/(mK) [21,41].

Regarding the temperature difference between the wall and the ambient gas phase, experiments with falling films heated from below show that $\Delta T=0.5-10$ K is well within an achievable range [42], while for the heat transfer between the liquid and the ambient gas phase, $\alpha_g=500-2000$ W/(m^2 K) with the lower value of this range corresponding to a moderate heat transfer coefficient [43].

For the precursor layer thickness, unless stated explicitly otherwise, we choose $h_*=0.2$. Then, if the dimensional precursor layer thickness is from $\tilde{h}_*=100$ nm to 10 μm (see, e.g., [21,37])—a tilde is introduced to distinguish between dimensional and dimensionless precursor layer thickness—the dimensional mean film thickness is from $h_0=500$ nm to 50 μm. Hence, if $\tilde{h}_*$ is in the lower end of the range of dimensional precursor layer thicknesses, then the flows considered here correspond to ultrathin films in the nanoscale regime with characteristic thicknesses of the order of 10^4 Å.

Regarding the dimensionless intermolecular force parameter A, Schwartz *et al.* [36,37] have performed a force balance in the neighborhood of the apparent contact line for a static equilibrium surface and showed that $A=\{(n-1)(m-1)/[2\tilde{h}_*(n-m)]\}\sigma_a(1-\cos\theta_e)$ where θ_e is the apparent equilibrium contact angle. Hence, A can be directly related to the wettability characteristics of the liquid-solid pair. Using the definition of the Bond number in Sec. II B, the dimensionless intermolecular force parameter can be written as $B=\{(n-1)(m-1)/[2(n-m)]\}(1-\cos\theta_e)[1/(\mathrm{Bo}h_*)]$. Following Schwartz *et al.* [36,37] and Teletzke *et al.* [44] we choose the values $(n,m)=(3,2)$ so that $B=5(1-\cos\theta_e)/\mathrm{Bo}$. With respect to the static contact angle θ_e, for water on highly hydrophilic surfaces and silicone oil on Perspex glass $\theta_e\lesssim1°$ [45] while for silicone oil on Pyrex $\theta_e\sim5°$ [46].

The above dimensional quantities then give the following wide ranges of dimensionless groups for water and silicone oil 50 cS both at 25 °C: $\mathrm{Ma}=1-2.9\times10^5$, $\mathrm{Bo}=4\times10^{-8}-1.2\times10^{-3}$, $\mathrm{Bi}=4.2\times10^{-4}-0.7$, and $B=0.6-1.9\times10^4$ (assuming $\theta_e=1°$). The extrema of these ranges vary by several orders of magnitude primarily due to the variation of h_0 by two orders of magnitude. Further, a typical range of values of the film parameter is $\epsilon=0.01-0.1$ (see, e.g., [43]). From the definitions of the modified parameters in Sec. II B, $\mathrm{Bo}'=\mathrm{Bo}/\epsilon^2$, $\mathrm{Ma}'=3\mathrm{Ma}\,\mathrm{Bo}'$, and $B'=B\,\mathrm{Bo}'$, we then have the following wide ranges for these parameters: $\mathrm{Bo}'=4\times10^{-6}-12$, $\mathrm{Ma}'=1.2\times10^{-5}-10^7$, and $B'=2.4\times10^{-6}-2.3\times10^5$.

As an example assume that the working liquid is water at 25 °C with a mean film thickness $h_0=50$ μm, temperature difference between the wall and the ambient gas phase $\Delta T=0.5$ K, and the relatively high heat transfer coefficient $\alpha_g=2000$ W/(m^2 K). We then have $\mathrm{Ma}=1.0$, $\mathrm{Bo}=4\times10^{-4}$, $\mathrm{Bi}=0.17$, and $B=1.9$ (assuming a highly hydrophilic surface with $\theta_e=1°$). These values are consistent with the orders-of-magnitude assignments Ma, $B=O(1)$, Bi at the most $O(1)$, and $\mathrm{Bo}=O(\epsilon^2)$ made in Sec. II C for the derivation of the long-wave model in Eq. (12).

IV. RESULTS

We solve numerically Eq. (12) by imposing periodic boundary conditions in an extended square domain $L\times L$ (sufficiently large for the instability to be seen) with periodic topography and by employing a global Fourier spectral expansion in both coordinates x and y. Details of the numerical scheme are given in the Appendix. The initial condition in all cases is white noise of maximum amplitude 0.05. The accuracy of the numerical scheme was determined by variation of the number of harmonics, time step sizing and by checking that $\int\int_{L\times L}h(x,y,t)dxdy$ is constant in time, a property that is guaranteed from Eq. (12) for periodic boundary conditions. The maximum computational domain used is $L\times L=100\times100$ while in all cases we found that a total of 48×48 real harmonics was large enough to provide us with sufficient accuracy. We have successfully used a similar numerical scheme before to investigate the dynamics of 3D solitary pulses in falling liquid films [47–49].

In our computations we set $\mathrm{Ma}=15$, $\mathrm{Bi}=0.1$, and Bo and B are varied in the regions [0, 0.7] and [1, 30], respectively, consistent with the ranges of parameter values in Sec. III [recall that primes have been dropped in the final evolution equation (12)]. Finally, as we pointed out in Sec. III for the dimensionless precursor film thickness we take the value $h_*=0.2$ unless stated explicitly otherwise.

A. 2D flows

Figure 2 depicts the evolution on a topographical substrate in the shape of a single harmonic of amplitude 0.1 and in a domain equal to the domain of the harmonic. The evolution is characterized by a slow relaxation process with continuous coalescence of drops (coalescence events occur throughout the topography including the peaks and depressions) starting from three drops at small times and ending up with just a single drop that survives at large times. Further, decreasing the amplitude of the topography to values smaller than 0.1 in Fig. 2 does not change the main characteristic of the interfacial evolution—i.e., the formation of a single drop in the trough of the topographical substrate.

At very small times the evolution is characterized by the formation of a number of point holes (e.g., three for the evolution in Fig. 2) due to the Marangoni instability. The minima of these holes can reach values smaller than h_* (as small as 0.15) but they subsequently increase to reach h_*. The larger the intermolecular force parameter B, the closer the minima are to h_*. The minima then start to flatten out, forming the precursor layer, while at the same time small satellite drops form at the minima. Eventually these drops drain to the surrounding liquid and the film reaches h_* (a

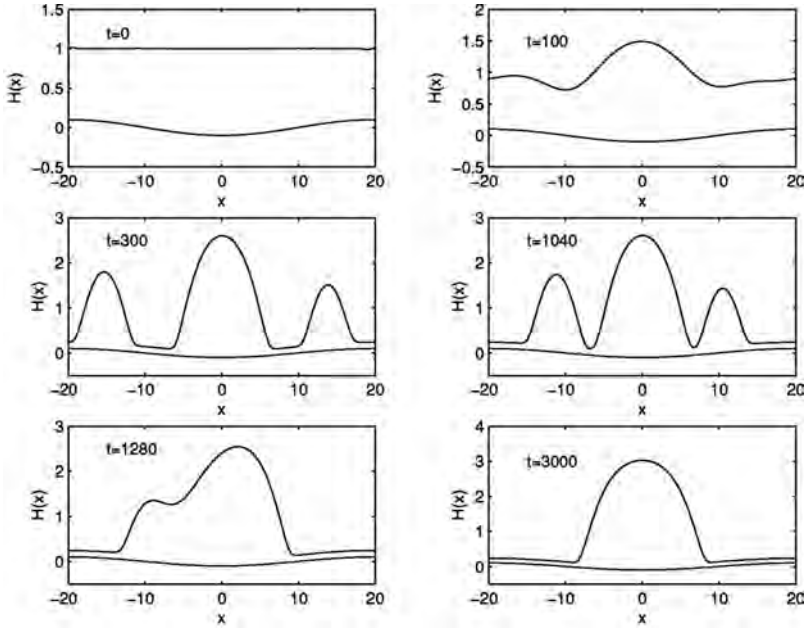

FIG. 2. 2D evolution for Bo=0.3 and $B=1$ on a topographical substrate with shape $s(x)=-0.1\cos(2\pi x/L)$ with $L=40$.

process which is accelerated by increasing B) while the holes open up leading to the formation of drops.

The mechanism for this drop formation process is the thermocapillary Marangoni effect: consider a flat interface with $H=1$ over a topographical substrate such as that in Fig. 2 for $t=0$. Points on the interface directly above the depression in topography are further from the topography compared to points directly above the peaks of the topography. As a consequence points above the depression in topography are colder compared to points above the peaks. This then creates a net surface tension gradient from the points above the peaks to those above the depression, leading to the formation of a drop over the depression. With multiple depressions (which are not necessarily the same), the liquid drains into the depressions and the final result of the evolution is a number of drops each of which is located in a depression, with the bigger drops located in the deeper depressions (which then contain more liquid). Hence, the dynamics of flow over a heated topographical substrate is substantially different to that over a heated planar substrate where the final result of the evolution is a single drop (or hole) [21].

Figure 2 also indicates that the smaller drops are moving slowly towards the bigger drop in the trough of the topography and eventually coalesce with this drop. The mechanism for this drop coalescence event is also the Marangoni effect which is what started the whole dynamics to begin with. Let us consider, e.g., the snapshot at $t=300$. Let us denote by 1 the peak of one of the two small neighboring drops, 2 the interface of the precursor film that separates the drops from the main drop, and 3 the peak of the main drop. Clearly $\sigma_2<\sigma_1$ and $\sigma_2<\sigma_3$. Hence, points from both areas 1 and 3 pull on the interface in area 2 but the surface tension gradient 2-3 is larger than 1-2 and wins over 1-2. The net effect is that the small drops are dragged towards the main drop: in essence this is equivalent to a "tug of war" between the drops as each of the small drops and the main drop pull on the precursor but the big one wins. Of course for this mechanism to be effective it is essential that we have a prewet substrate as the precursor film provides the connecting medium through which the drops can communicate.

This coalescence process is assisted by gravity since motion of the small neighboring drops towards the troughs of the topography lowers their potential energy thus speeding up their motion. We have repeated the computation in Fig. 2 in the absence of gravity—i.e., for Bo=0—as shown in Fig. 3. The coalescence process is now a lot slower and takes more than 3000 time units for the small neighboring drops to come to a close proximity with the main drop as in Fig. 2 for $t=1040$. Gravity affects not only the rate by which the small drops move towards the bigger ones but also the shape of the final drop, as expected: for Bo=0 the drop is more pointed and slender while for Bo$\neq$0 the drop is more rounded with a flatter peak and a height smaller to that for Bo=0 (but with the same volume due to conservation of mass for periodic boundary conditions).

The bigger drops in neighboring troughs of the topography do not seem to coalesce with each other. For a regular topography such as that in Fig. 2 this is obvious as the drops in the troughs have the same height. If neighboring troughs are different, coalescence between the main drops in the troughs would involve that the drops climb over the ridges that separate them. At the same time the distance between the main drops weakens the Marangoni effect. In the absence of gravity it is possible that drops in deeper depressions attract those in more shallow depressions leading to coalescence events between drops in different depressions, but this is a process that would take a very long time.

With respect to the value $h_*=0.2$ of the precursor film, it was found to be sufficient to resolve the main dynamic characteristics of the evolution of the interface. Smaller values of h_* have also been tested; e.g., we found that by decreasing h_* from 0.2 to 0.1 the main features of the evolution are qualitatively the same; i.e., the amplitude and position of the drops and the number of drops at a given instance in time is practically the same while the final evolution remains unaltered with the main drop in the trough of the topography and

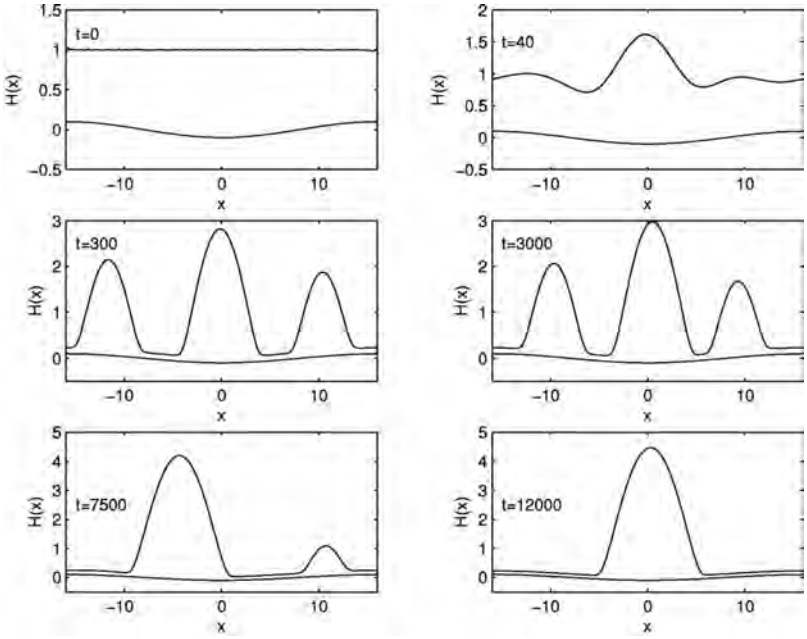

FIG. 3. 2D evolution for the conditions in Fig. 2 but Bo=0.

always in the same position and its height practically the same—a small increase occurs by decreasing h_* due to conservation of mass for periodic boundary conditions. In addition, the value of h_* chosen here is less than 10% of the maximum amplitude of the final drop in Figs. 2 and 3 which is close to 3 and in excess of 4, respectively.

Note that the general topological structure of the initial evolution of the interface is similar to that observed in the time-dependent computations by Kabova *et al.* [32] but for a dry substrate. As a result the temporal evolution obtained by these authors was restricted due to rupture which occurred when the minimum film thickness became very small. In fact, continuing the computations at this point typically leads to unphysical negative values for the film thickness much like with the case of a flat substrate [18]. In the present study, instead of rupture and completely dry domains the solid substrate is always covered by a thin precursor film as the disjoining pressure prevents the film from breaking. This allows the study of the long-time evolution of a film unstable due to the Marangoni effect induced by a heated topographical substrate.

Figure 4 depicts the evolution on a topographical substrate in the shape of a single harmonic of amplitude 0.3 and in a domain equal to the wavelength of the harmonic. Now Bo is larger than that in Fig. 2, corresponding to a more stable situation to that in Fig. 2. As a consequence the evolution slows down significantly and the time necessary to establish a single drop is more than twice as long as in Fig. 2. Further, due to the larger domain in Fig. 4, we have four drops instead of three at small times.

We note that for a flat heated substrate the parameter that determines the onset of the linear instability is Ma Bi/

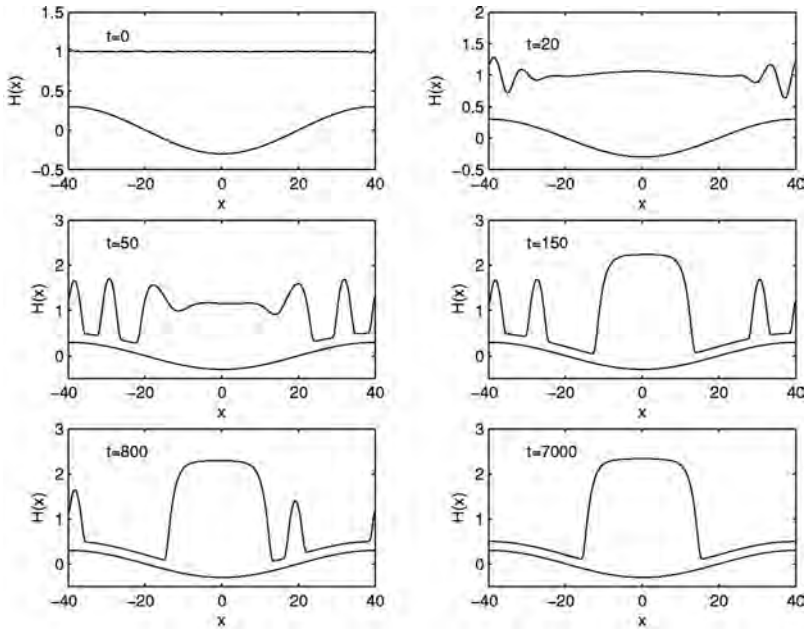

FIG. 4. 2D evolution for Bo=0.7 and $B=10$ on a topographical substrate with shape $s(x)=-0.3\cos(2\pi x/L)$ with $L=80$.

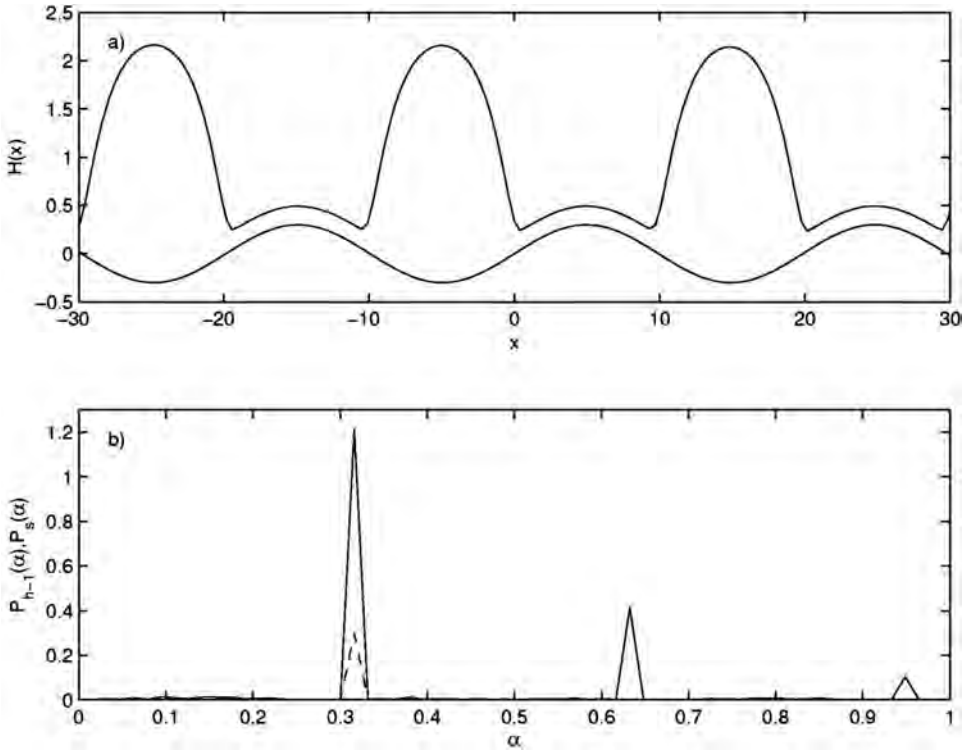

FIG. 5. (a) Free surface snapshot for Bo=0.7 and $B=10$ at $t=10\,000$ on a topographical substrate with shape $s(x)=0.3\sin[3(2\pi/L)x]$ with $L=60$. (b) Power spectrum for $h-1$ (solid line) and s (dashed line) as a function of wave number α.

$[2(1+\mathrm{Bi})^2]-\mathrm{Bo}$ so that the trivial flat-film solution is unstable if and only if this parameter is >0 [21]. For the parameter values in Fig. 4 this parameter is <0 and yet the system is unstable. This demonstrates the destabilizing role of the topography due to its coupling with the Marangoni effect: recall from our earlier discussion on the mechanism of the instability that an initially flat film with $H=1$, such as that in Fig. 4 for $t=0$, contains alternating regions with relatively cold and hold fluid over the troughs and peaks of the topography, respectively. Hence, in contrast to free-surface thin-film flows over topography with a mean flow driven by a body force where the topography stabilizes the flows, in our case it has a destabilizing influence (through its coupling with the Marangoni effect). On the other hand, for $\mathrm{Ma}=0$, the hydrodynamics is decoupled from the heat transport process and the flat interface $H=1$ is stable (note that unlike the flat-substrate case, $h=1$ is not a solution).

Figure 5(a) shows the large-time evolution on a topographical substrate in the shape of a single harmonic of amplitude 0.3 but now in a domain three times the wavelength of the harmonic. Figure 4(b) shows the power spectrum of the free surface and topography in Fig. 4(a). The power spectrum has the typical structure one would expect from a nonlinear signal and is characterized by a dominant harmonic at a certain wave number and a superharmonic at a wave number roughly twice that of the dominant one. At earlier times, this superharmonic has a larger amplitude and hence higher "energy" due to the small drops which are still present in the domain between the main drops in the troughs of the topographical substrate. Clearly, there is a strong correlation between h and s.

B. 3D flows

Figure 6 depicts the pattern formation process in 3D flow over three holes in topography. The topographical shape is given by

$$s(x,y)=\sum_{i=1}^{3}\left\{\frac{1}{2}-D\left[\frac{1}{2}-\frac{1}{\pi}\tan^{-1}\left(\frac{r_i-R}{\delta}\right)\right]\right\},$$

$$r_i=\sqrt{(x-x_{0_i})^2+(y-y_{0_i})^2}, \tag{13}$$

where D, R, and (x_{0_i},y_{0_i}) denote the hole depth, radius, and location of the ith hole, respectively. δ is a parameter that controls the steepness of the hole so that the walls of the holes become increasingly sharp for small δ. We set $D=0.5$, $R=7$, and $\delta=0.7$.

For very small times we observed the development of a number of point holes due to the Marangoni instability. Some of these point holes turn into line holes which in turn join up to form drops. At later times the liquid forms circular rings above the edges of the holes. A cross section of these rings has a shape similar to that of the *capillary ridge* observed for 2D flows over a step-down in topography driven by a body force [25–29]. In these flows, the formation of the ridge is a manifestation of the capillary pressure gradient induced by the substrate curvature and the profile for the free-surface results from the competition between the substrate feature, which creates an interfacial shape that is an impression of the topography, and surface tension which tends to flatten the free surface. References [26,29,30] performed a detailed stability analysis of the spectrum of the linearized operator that governs the evolution of infinitesimal disturbances in the

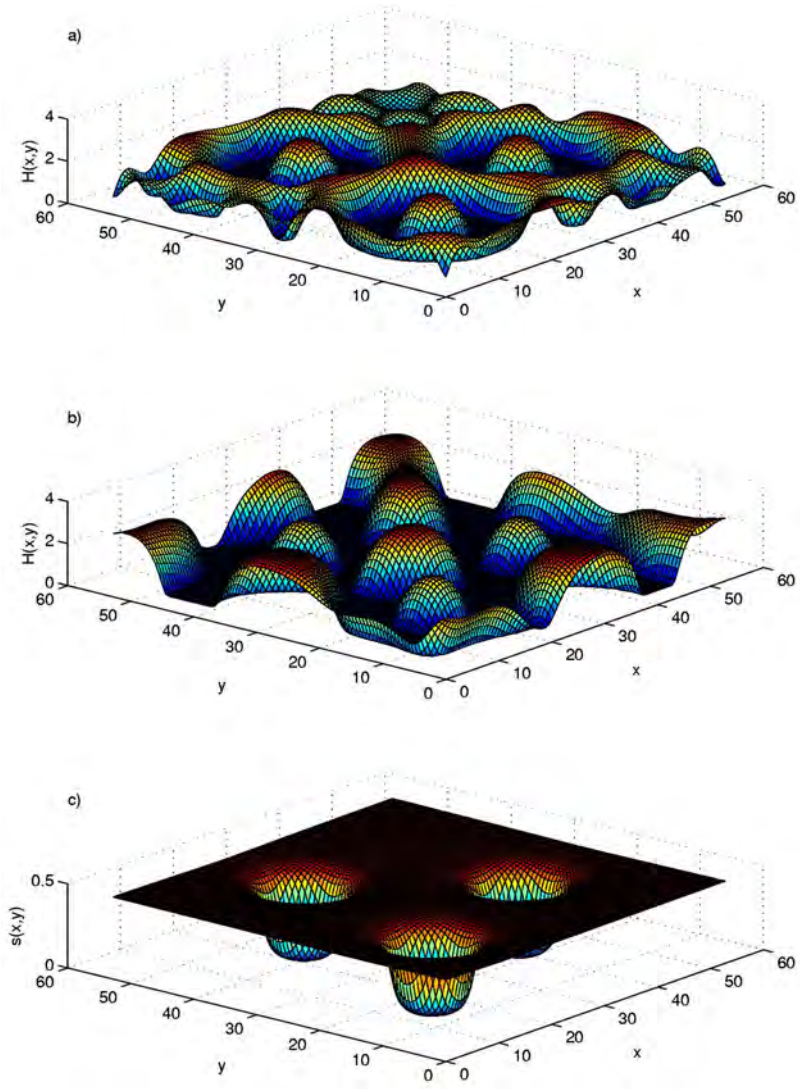

FIG. 6. (Color online) 3D evolution for Bo $=0.5$, $B=10$ over three holes in topography located at $(x_{0_1},y_{0_1})=(15,15)$, $(x_{0_2},y_{0_2})=(21,40)$, $(x_{0_3},y_{0_3})=(38,41)$ with $D=0.5$, $R=7$, $\delta=0.7$. (a) Free-surface snapshot at $t=20$. (b) Free-surface snapshot at $t=100$. (c) Topography.

transverse direction together with a nonmodal analysis of the linearized eigenvalue problem and demonstrated the strong stability of capillary ridges.

In our case, the rings/3D capillary ridges formed over the edges of the holes develop an instability which is already visible in Fig. 5(a) for $t=20$. This instability breaks the rings into drops as shown in Fig. 6(a) for $t=100$. These drops grow initially, as they are still connected to each other with relatively thick films, and hence it is easier for the liquid to drain from the rings into the drops it breaks into, rather than into the holes. Nevertheless, throughout the evolution liquid drains continuously into the holes and eventually for very large times the system will evolve into three drops situated within the holes.

Note that the drops forming from the rings over the edges of the holes initially have larger heights compared to the drops situated within the holes. But this should not be interpreted as the drops forming from the rings might contain more liquid than the holes. Recall that here we show the overall height $H=h+s$. The deviation height for the drops within the holes might still be bigger to that for the drops forming on the edges of the holes and in this case the holes do contain more liquid.

Figure 7 depicts the evolution of the interface on a "quasirandom" topography. At $t=300$ most of the liquid mass is concentrated in the troughs of the topography, and in fact at this instance in time the interface is close to its steady state for large times. The smaller drops surrounding the bigger drops situated in the troughs will eventually drain into the troughs. The size of these final drops depends on the troughs they are situated in with the bigger drops appearing in deeper troughs. In addition, much like the 2D case discussed earlier, drop coalescence occurs throughout including the crests and troughs of the topography.

Further insight into this coalescence process can be gained by examining the number of drops N as a function of time as shown in Fig. 8. The plot starts from $t=20$ as for small times it is difficult to identify well defined drops. As time progresses drops coalesce and their number decreases. Any drop with a deviation height h smaller than $1/4$ of that of the biggest drop in the domain is not counted. These uncounted drops will eventually coalesce with bigger drops. The local increases in N shown in the figure are due to the fact that the amplitude of small, initially uncounted, drops can increase after coalescence with bigger drops and hence they are counted. This increase happens right before the

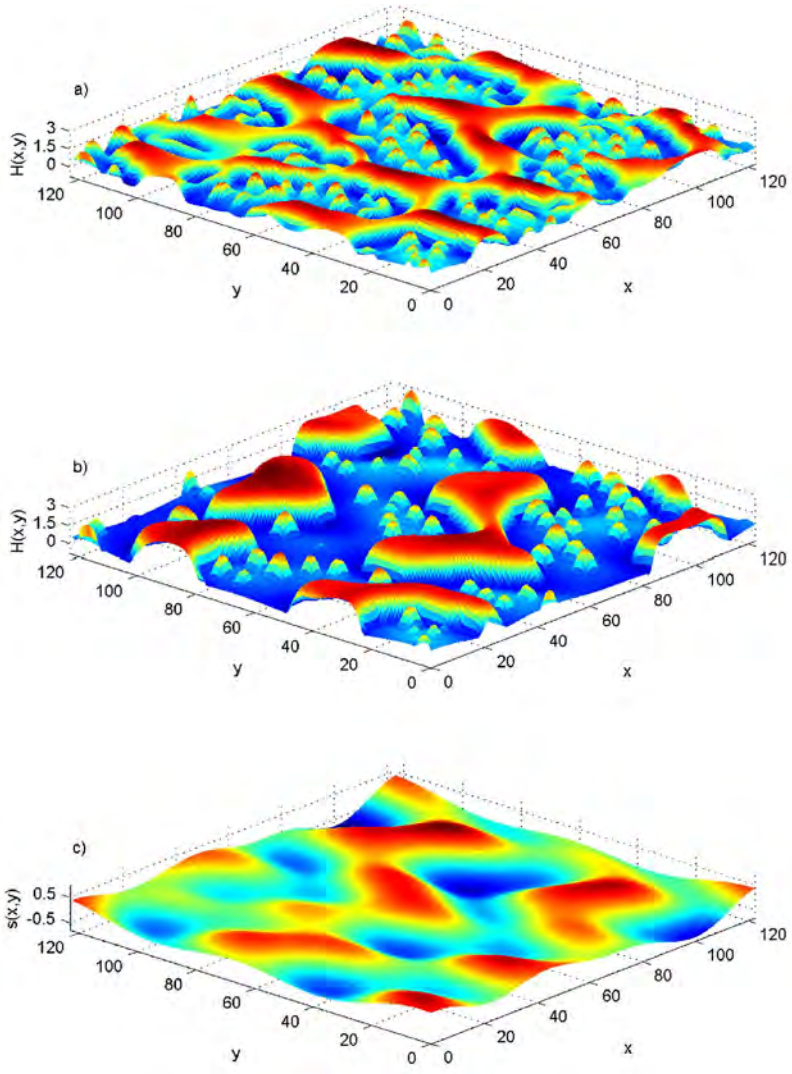

FIG. 7. (Color online) 3D evolution for Bo $=0.5$, $B=10$, $h_*=0.15$ over quasirandom topography with shape $s(x,y)=0.1\sin(2y)+0.3\cos(2y)\times\sin(x)+0.2\cos(y)\cos(3x)+0.25\sin(2y)\sin(4x)+0.23\cos(2y)$. (a) Free surface at $t=30$. (b) Free surface at $t=300$. (c) Topography.

small drops are completely absorbed by the bigger drops. When all such coalescence events are complete, the number of drops decreases again. Eventually this coarsening dynamics terminates at large times as is evident from Fig. 8 where the number of drops appears to asymptote to a certain value. This limit is equal to the number of troughs in the topograph. For the particular numerical experiment in Fig. 8 we have 36 troughs.

In Fig. 9 we plot the pair correlation functions $g(r)$ for the local maxima of the free surface (since the time is sufficiently long these maxima coincide with the peaks of the drops in the troughs) and the local minima of topography (troughs) for the parameter values in Fig. 8 and $t=300$. In general, this function is related to the probability of finding the center of an object at a distance r from the center of another object. These objects in the problem considered here are the troughs of the topography and the drops. The bigger the value of $g(r)$, the higher the probability to find objects at a distance r. As an example the peak at $r\sim 35$ for the topography pair correlation function in Fig. 9 implies that there is a large probability of finding two minima in topography separated by a distance of 35 units.

This function is computed by the following algorithm: (i) We choose a value of Δr. (ii) We consider every object we have in turn and count all objects that are a distance $r+\Delta r$ away from the object we are considering. These objects are in a cylindrical shell of thickness Δr surrounding the reference object. (iii) We divide the total count by N, the number of reference objects we considered. (iv) This number is then divided by the area of the shell, $\pi(r+\Delta r)^2-\pi r^2$. This accounts for the fact that as r gets larger, there are simply more objects with the given separation. (v) Further, we normalize this number with the "objects number density" defined as $N/$(area). This ensures that $g(r)\equiv 1$ for a cluster of objects without any structure (i.e., a random configuration).

The pair correlation analysis shows a strong correlation between topography and the interface at large times. In particular the pair correlation functions for the local maxima of the interface and the local minima of the topography have maxima at roughly the same locations indicating that most likely the distances between the local minima of the topography and local maxima of the interface are the same.

C. Chemically heterogeneous substrates

Chemically heterogenous substrates can be modeled by allowing the intermolecular parameter B to be spatially vary-

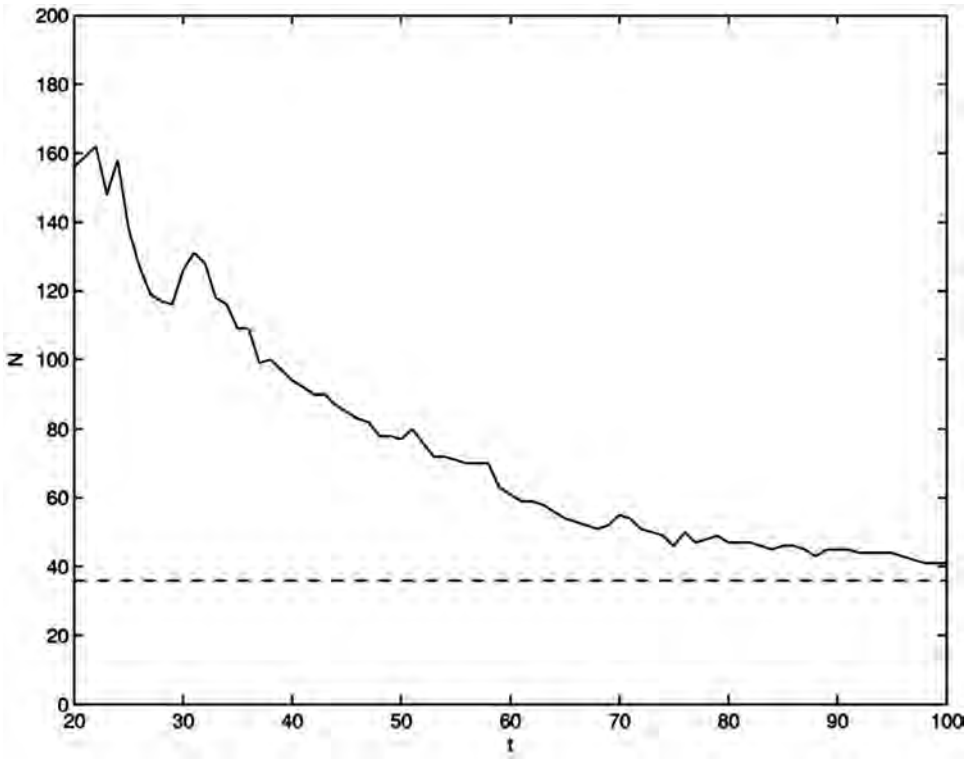

FIG. 8. Number of drops N as a function of time for Bo=0.7, $B=10$ on a topography with shape $s(x,y)=0.3\sin[6(2\pi/L)x]\times\sin[3(2\pi/L)y]$ with $L=160$. The dashed line indicates the number of troughs in topography (=36).

ing. This would be the case when, e.g., the substrate is coated with areas of different wetting characteristics. Previous studies have focused on isothermal films on chemically patterned flat substrates [50–54], films climbing up chemically patterned vertical flat substrates due to a temperature gradient on the substrate [55], and gravity-driven thin-film flow on a heterogeneous inclined substrate (the heterogeneities are modeled by perturbing the precursor film ahead of the macroscopic front) [56].

Figure 10 shows the evolution on a flat uniformly heated substrate with $B=10$ except for a heterogeneity that consists of a diagonal strip with $B=30$. The liquid is moving away from the "affected," area and provided that the width of this stripe is not too large, there are no drops forming there (for

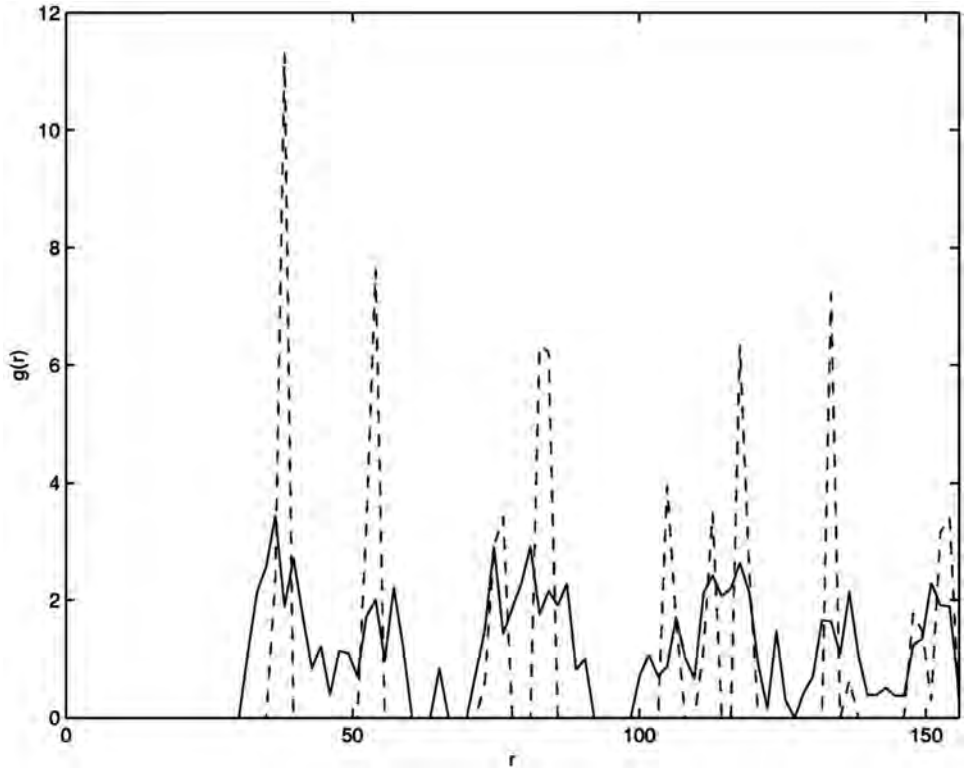

FIG. 9. Pair correlation function for the same parameters with Fig. 7 and $t=300$. The topography shape is $s(x,y)=0.3\sin[3(2\pi/L)x]\cos[3(2\pi/L)y]$ with $L=120$. This topographical feature has 18 identical troughs. Solid line: local maxima of drops. Dashed line: local minima of topography.

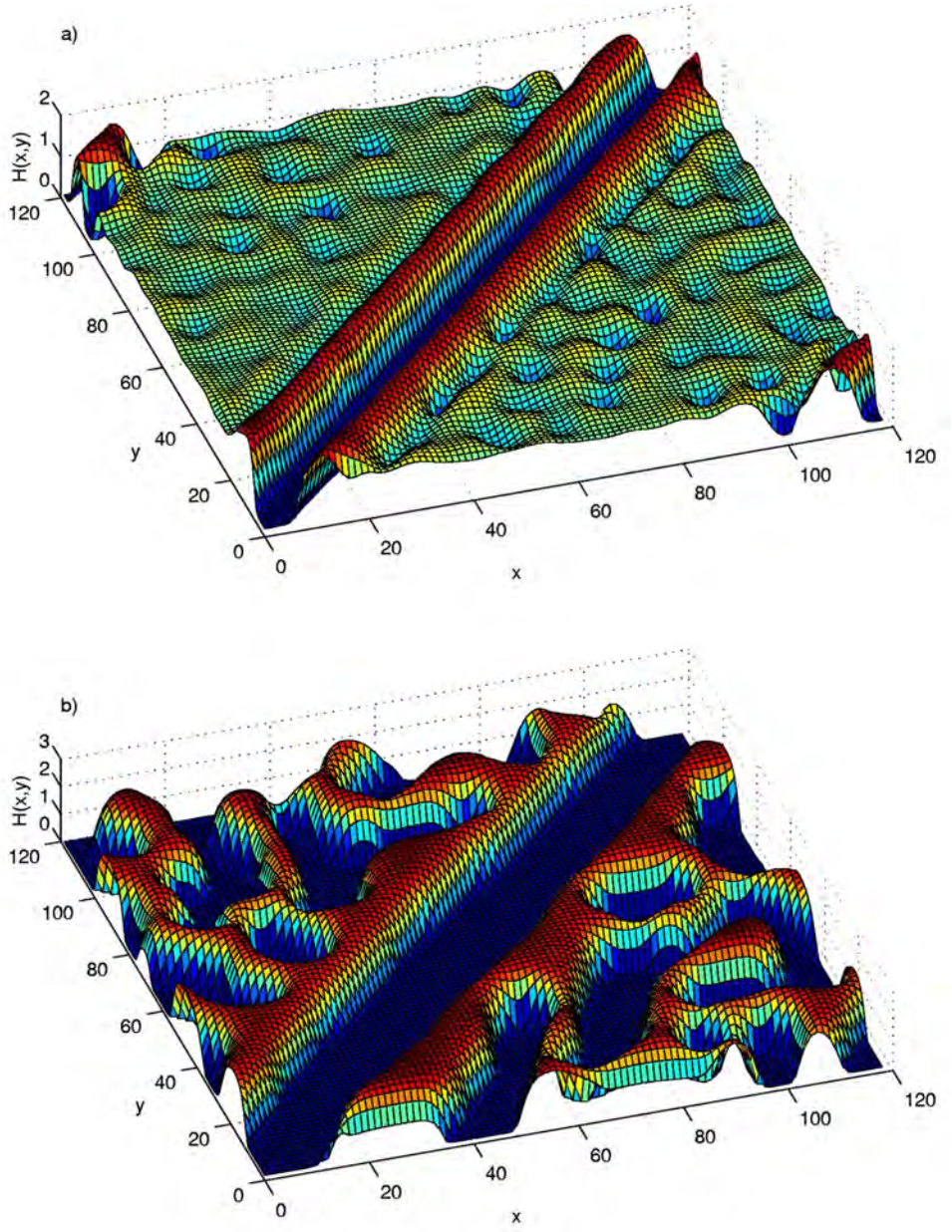

FIG. 10. (Color online) Spreading over a chemically heterogeneous uniformly heated flat substrate with Bo=0.7. The intermolecular parameter $B(x,y)$ is chosen to be 10 everywhere except a diagonal stripe of width $\sqrt{10}$ where it is equal to 30. (a) $t=20$. (b) $t=150$.

sufficiently large widths drops will form on the heterogeneity). Away from the heterogeneity the dynamics is similar to that observed in 3D flows over uniformly heated flat substrates [21].

We now turn to the interaction between topography, Marangoni effect, and chemical heterogeneities. In particular, we wish to examine the possibility of utilizing the wettability contrast as a control parameter for the drop formation process in the troughs of the topography. As the computation in Fig. 10 indicates the liquid drains away from the areas of large B. On the other hand, the computations over chemically homogeneous substrates discussed earlier indicate that the liquid drains into the troughs of the topography. Hence, increasing the intermolecular parameter B in the troughs might prevent the liquid from organizing into drops there.

Figure 11 shows the evolution over a chemically patterned substrate with $B=10$ everywhere except a rectangle where $B(x,y)=10-70\cos[2(2\pi x)/L]\sin[3(2\pi y/L)]$. The topographical feature has 18 identical troughs. The spatial variation of the intermolecular parameter B has a significant influence on the free surface even at small times. Eventually the liquid drains out of the chemically heterogeneous trough resulting in a film that conforms closely to the topography with a thickness $\sim h_*$ in the area of the heterogeneity.

V. SUGGESTIONS FOR PHYSICAL EXPERIMENTS AND POSSIBLE APPLICATIONS

The study presented here can be used as a basis for the design of experiments on the dynamics of thin films driven by both the thermocapillary Marangoni effect and substrate curvature.

The simplest possible such experiment would be the behavior of a thin film on a regularly corrugated substrate—e.g., the situation depicted in Fig. 5. For this purpose a sample consisting of a thin (nonvolatile) film deposited onto

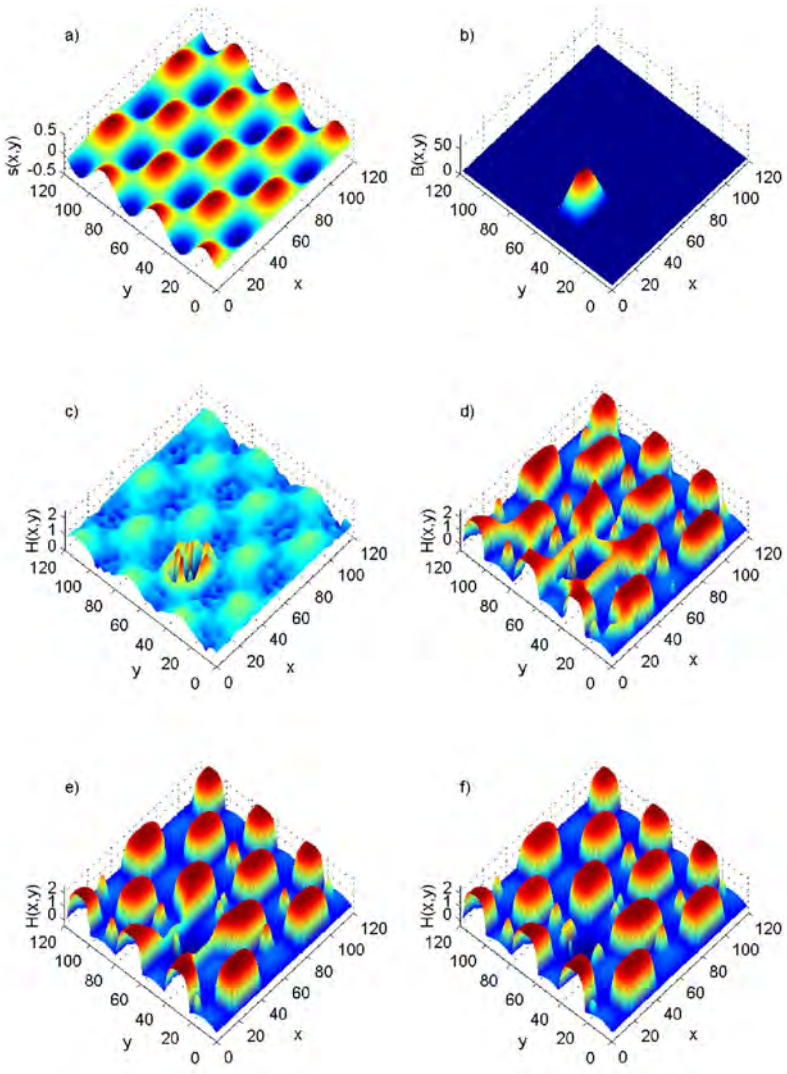

FIG. 11. (Color online) Spreading over a chemically heterogeneous topographical substrate with Bo=0.7. (a) Topography shape given by $s(x,y)=0.3\cos[2(2\pi/L)x]\sin[3(2\pi/L)y]$ with $L=120$. This topographical feature has 18 identical troughs. (b) Chemical heterogeneity with shape $B(x,y)=10-70\cos[2(2\pi/L)x]\times\sin[3(2\pi/L)y]$ with $(x,y)\in(15,40)\times(45,60)$. Outside this rectangle $B(x,y)=10$. (c), (d), (e), (f) Free-surface snapshots at $t=5,100,300,500$, respectively.

the corrugated substrate would have to be heated from below to a certain temperature followed by monitoring of the interface evolution as a function of time. The theory presented here suggests that for sufficiently large times the film will break into (linear in the transverse direction) channels following the grooves of the substrate. A number of experimental predictions for this setting can be made from our study. These include typical times to form drops in the grooves of the topography, the drop amplitudes and shapes for a given topography/shape of grooves, and the amount of liquid that will accumulate in the grooves.

To fix ideas let us assume that the liquid used in the "experiment" of Fig. 5 is silocone oil 50 cS at 25 °C whose physical properties are given in Sec. III. The dimensionless parameters used in the computation of Fig. 5 are $\mathrm{Bo}'=0.7$, $B'=10$, $\mathrm{Ma}'=15$, and $\mathrm{Bi}=0.1$. We first estimate the film parameter ϵ: from $\epsilon=h_0/\ell$, $\ell\sim\tilde{L}$, and $L=\tilde{L}/h_0$ (again tildes are introduced to distinguish between dimensional and dimensionless quantities), we have $\epsilon=1/L=1/60\sim0.017$ where $L=60$ is the dimensionless wavelength of the topographical function in Fig. 5. From $\mathrm{Bo}'=\mathrm{Bo}/\epsilon^2$ we then have $\mathrm{Bo}\sim2.023\times10^{-4}$. But $\mathrm{Bo}=\rho g h_0^2/\sigma_a$ which can be used to obtain the mean film thickness $h_0=\sqrt{\mathrm{Bo}\sigma_a/(\rho g)}\sim20$ μm within the range of film thicknesses given in Sec. III.

From the definition now of the modified Marangoni number, $\mathrm{Ma}'=3\mathrm{Ma}\,\mathrm{Bo}'$, we obtain $\mathrm{Ma}=7.14$. The definition then $\mathrm{Ma}=\gamma\Delta T/(\mu u_0)$ of the Marangoni number where the characteristic velocity is given by $u_0=gh_0^2/\nu$ can be used to estimate the temperature difference across the film, $\Delta T=\mathrm{Ma}(\rho g h_0^2/\gamma)\sim0.5$ K, at the lower end of the range of temperature differences given in Sec. III.

With h_0 known we can use the value of the Biot number used in the computation of Fig. 5 to estimate the heat transfer coefficient at the liquid-gas interface. From the definition $Bi=\alpha_g h_0/\lambda$ we obtain $\alpha_g=750$ W/(m^2 K), close to the lower end of the range of heat transfer coefficients given in Sec. III.

Further, from the definition of the modified intermolecular force parameter, $B'=B\mathrm{Bo}'$, we obtain $B=14.3$. Hence, from the expression $B=5(1-\cos\theta_e)/\mathrm{Bo}$ given in Sec. III we have $\theta_e\sim2°$. The corresponding substrate material then must have wettability characteristics close to that of Perspex glass—recall from Sec. III that solicone oil 50 cS almost completely wets this type of glass as $\theta_e\lesssim1°$.

The final maximum drop height can also be estimated: with $H_{\max}\sim2.1$ from Fig. 5 and $H_{\max}=\tilde{H}_{\max}/h_0$, we obtain $H_{\max}\sim40$ μm. Another experimental quantity of interest

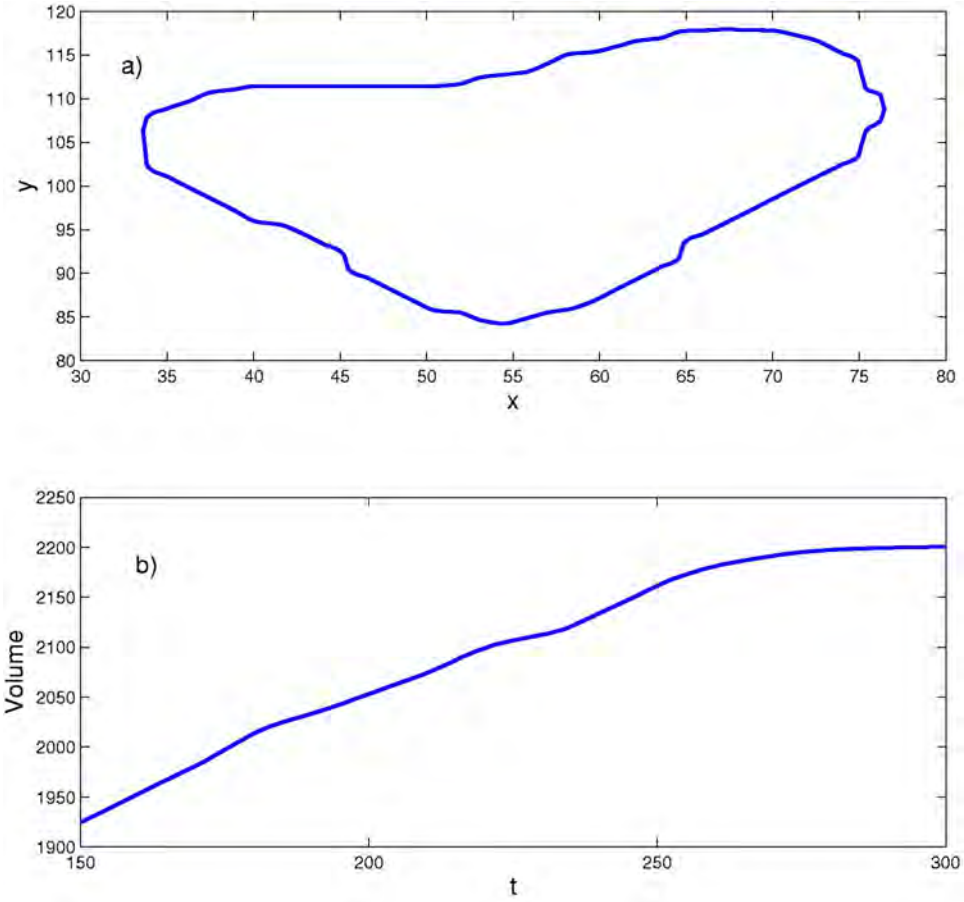

FIG. 12. (Color online) Draining process into the topography hole centered at $(x,y)\sim(60,100)$ in Fig. 7. (a) Border of the drop formed in the hole at $t=300$—see Fig. 7(b). (b) Volume of the drop formed in the hole as a function of time.

would be the time it takes to form the drops in the grooves of the topography. Figure 5 shows a snapshot of the evolution at the very large time, $t'\sim 10\,000$. Our computations indicate that at $t'\sim 1000$ the free surface is already close to its final configuration. From $t'=t/(3\mathrm{Bo}')$ we then have $t\sim 2100$. But $t=(\epsilon u_0/\ell)\tilde{t}\equiv[\mu/(\epsilon^2\rho g h_0)]t$ or $t\sim 22.3$ days. To reduce this time one can explore different possibilities—e.g., increase the modified Bond number Bo' as Figs 2 and 3 clearly indicate. Since $\mathrm{Bo}'=\mathrm{Bo}/\epsilon^2$ to reduce Bo', we can either increase ϵ (via changing the design of the topography and decreasing L) and/or decrease Bo. But $\mathrm{Bo}=\rho g h_0^2/\sigma_a$. For a fixed liquid, Bo decreases when h_0 decreases.

With regards to the amount of liquid filling the holes of the topography this can be estimated by simply integrating the interfacial height over the area Ω covered by the hole, $\int\int_\Omega h(x,y,t)dxdy$. Figure 12 shows one such computation for the situation depicted in Fig. 7. The figure monitors the draining process into the topographical hole centered at $(x,y)\sim(60,100)$ in Fig. 7(c). Figure 12(a) depicts the border of the liquid drop for $t=300$ over the hole, i.e., the drop in Fig. 7(b) centered at the same location with the hole and Fig. 12(b) monitors the volume of the drop as a function of time. Clearly for large t the volume seems to approach the asymptotic value ~ 2200.

The theoretical results presented here show that the competition between the thermocapillary Marangoni effect, topographical substrate curvature, and intermolecular forces might serve as a means of controlling the morphology of dewetting films. The subsequent dewetting events leading to the formation of big drops in the troughs of the topography offer an attractive self-organizational process for guiding the instabilities on the surface of the film to form structures from the nanometer to the micrometer scale. This method of structuring films via mimicking the substrates in which the films are deposited might have applications in several areas ranging from microfluidics to biological settings. Indeed, one possibility might be to utilize topographical substrates to develop polymeric networks/circuits with electrically conducting polymers. Other possible applications might include microprinting/patterning (e.g., pattern replication through deposition of liquids in a regular manner determined by the template) and directing biological cell populations along ridges of liquids. The combination of topography and chemical heterogeneities would offer even greater control and ordering of the resulting structures.

On the other hand, in some situations a completely leveled surface might be desirable—e.g., in leveling/planarization of topography in fabrication steps of microelectronic components [57–59]. The current method to achieve leveling relies on allowing the film to level following spin coating of the topographical substrate. Our study shows that the wettability characteristics of the solid-liquid pair are a crucial factor for the spreading dynamics of thin films on topographical substrates. It also indicates that by carefully choosing Bo and Ma, via, e.g., tuning the average film thickness h_0, we can avoid the thermocapillary Marangoni instability and obtain a leveled surface (increasing h_0 increases

Bo and decreases Ma, both having a stabilizing influence on the film). On the other hand, for sufficiently small film thicknesses—i.e., sufficiently small Bo and Ma—the instability cannot be prevented. Nevertheless, by carefully varying the wettability characteristics locally the fluid can be moved out of the topographical holes and redistributed with a view of leveling the free surface. However, we are still some way off from describing leveling of microelectronic components. Indeed, in applications the working fluids are frequently polymeric solutions and not pure liquids while leveling of uneven substrates and spin coating involves additional complex processes such as solvent evaporation. Hence, the model presented here would have to be modified for a polymeric solution by decomposing the stress tensor into a Newtonian solvent contribution and a polymeric one (given by, e.g., an Oldroyd-B constitutive equation). We would also have to take onto account the increase of viscosity due to solvent evaporation and the decrease of the evaporation rate as the solution dries.

VI. SUMMARY

We have examined numerically the dynamics of free-surface thin-film flows over uniformly heated topographical substrates. Through a series of 2D and 3D computations we demonstrated that the evolution is typically characterized by accumulation of liquid in the troughs of the topography because that is where the surface tension is higher to begin with (and remains higher). The accumulated fluid assumes the form of big drops surrounded by small drops which they become "attracted" to the big drops through the Marangoni effect. This leads to a continuous coalescence process until no more small drops surrounding the main drops are present. The final result of this slow relaxation process is a steady state that consists of a series of drops in the troughs of the topography. These final equilibrium drops are a consequence of the competition between the thermocapillary Marangoni effect which tries to break the film, substrate curvature which induces an additional capillary pressure, and intermolecular forces that stabilize a film of thickness h_*. The drop formation process can be prevented by a local variation of the intermolecular force parameter.

There are a number of interesting questions related to the analysis presented here. For example, it would be interesting to use elements from optimal control theory to vary dynamically $B(x,y,t)$ with the view to controlling the interface so that it conforms closely to the topography throughout the domain or to coat a desired pattern. It would also be interesting to investigate the case of spatially varying heating with $T_w = T_w(x,y)$, again with the view of controlling the interface as was done in Ref. [28] to minimize the capillary ridges for 2D flows over topography driven by a body force.

It is important to point out here that a detailed bifurcation analysis of all possible steady states and their stability was beyond the scope of the present study. In particular, we note that preliminary analysis of the eigenvalue problems governing the stability of single drops such as those seen for large times in Figs. 2, 3, and 4 indicates that these eigenvalue problems are nontrivial and have both discrete and essential spectra (see, e.g., Refs. [9,26]). Of particular interest would also be the development of a coherent structures theory to analyze the interaction of drops (see [49] for a theory describing the interaction of 3D solitary pulses) and determine precisely the conditions that lead to drop coalescence. We shall examine these and related problems in a future study.

ACKNOWLEDGMENT

We thank Professor A. Oron and Dr. Ralf Seemann for useful discussions and suggestions. We acknowledge financial support from Dow Benelux B.V., an Overseas Research Scholarship award, and the Engineering and Physical Sciences Research Council of England through Grant Nos. GR/S01023 and GR/S49520.

APPENDIX

The numerical method for the solution of Eq. (12) is based on a trigonometric Fourier series of the form

$$\begin{aligned} f(x,y,t) = A_{0,0} &+ \sum_{k=1}^{N} [A_{2k-1,0}\cos(kx) + A_{2k,0}\sin(kx)] \\ &+ \sum_{l=1}^{M} [A_{0,2l-1}\cos(ly) + A_{0,2l}\sin(ly)] \\ &+ \sum_{k=1}^{N}\sum_{l=1}^{M} [A_{2k-1,2l-1}\cos(kx)\cos(ly) \\ &+ A_{2k-1,2l}\cos(kx)\sin(ly) + A_{2k,2l-1}\sin(kx)\cos(ly) \\ &+ A_{2k,2l}\sin(kx)\sin(ly)], \end{aligned} \tag{A1}$$

where f is any function of $h(x,y,t)$, $s(x,y)$, and their derivatives. The coefficients of this Fourier expansion are time dependent.

Assume for simplicity that $h(x,y,t)$ and $s(x,y,t)$ are periodic in both spatial directions with a period equal to 2π or, alternatively, utilize the coordinate transformation to $x \to x/[L/(2\pi)]$ and $y \to y/[L/(2\pi)]$ where L is the period in both the x and y directions, to convert the period of the two functions to 2π. We then rewrite Eq. (A1) as

$$\partial_t h = F(x,y,t), \tag{A2}$$

where

$$\begin{aligned} F(x,y,t) = &-\frac{1}{2}\mathrm{Ma}\,\mathrm{Bi}\,\boldsymbol{\nabla}\cdot\left(\frac{h^2}{(1+\mathrm{Bi}h)^2}\boldsymbol{\nabla}h\right) \\ &+ \mathrm{Bo}\,\boldsymbol{\nabla}\cdot(h^3\boldsymbol{\nabla}H) - \boldsymbol{\nabla}\cdot[h^3\boldsymbol{\nabla}(\boldsymbol{\nabla}^2 H + B\mathsf{P})]. \end{aligned}$$

By substituting now the Fourier decompositions of $h(x,y,t)$ and $F(x,y,t)$ into Eq. (A2) gives:

$$\partial_t \Bigg[AH_{0,0} + \sum_{k=1}^{N} [AH_{2k-1,0}\cos(kx) + AH_{2k,0}\sin(kx)] + \sum_{l=1}^{M} [AH_{0,2l-1}\cos(ly) + AH_{0,2l}\sin(ly)]$$
$$+ \sum_{k=1}^{N}\sum_{l=1}^{M} [AH_{2k-1,2l-1}\cos(kx)\cos(ly) + AH_{2k-1,2l}\cos(kx)\sin(ly) + AH_{2k,2l-1}\sin(kx)\cos(ly) + AH_{2k,2l}\sin(kx)\sin(ly)] \Bigg]$$
$$= AF_{0,0} + \sum_{k=1}^{N} [AF_{2k-1,0}\cos(kx) + AF_{2k,0}\sin(kx)] + \sum_{l=1}^{M} [AF_{0,2l-1}\cos(ly) + AF_{0,2l}\sin(ly)]$$
$$+ \sum_{k=1}^{N}\sum_{l=1}^{M} [AF_{2k-1,2l-1}\cos(kx)\cos(ly) + AF_{2k-1,2l}\cos(kx)\sin(ly) + AF_{2k,2l-1}\sin(kx)\cos(ly) + AF_{2k,2l}\sin(kx)\sin(ly)] \tag{A3}$$

and the Fourier-transformed equation is written in terms of the time-dependent coefficients $AH_{k,l}$ for $k=1,2,\ldots,N$, $l=1,2,\ldots,M$ of $h(x,y,t)$ and $AF_{k,l}$ for $k=1,2,\ldots,N$, $l=1,2,\ldots,M$ of $F(x,y,t)$ which are functions of $AH_{k,l}$ since $F(x,y,t)$ is a function of $h(x,y,t)$. After collecting the same harmonics we can decompose Eq. (A3) into $(2N+1)\times(2M+1)$ ordinary differential equations of the form

$$\partial_t AH_{k,l} = AF_{k,l}(AH_{i,j}), \tag{A4}$$

where $k=1,2,\ldots,N$, $l=1,2,\ldots,M$, $i=1,2,\ldots,N$, and $j=1,2,\ldots,M$.

The system in Eq. (A4) was marched in time using the IMSL solver DIVPAG based on Gear's method for stiff systems and with dynamic adjustment of the time step (it was typically varied between 10^{-5} and 10^{-2}). To compute the functions $AF_{k,l}(AH_{i,j})$ on the right-hand side of Eq. (A4), $h(x,y,t)$ is evaluated in every iteration of Newton's method in DIVPAG from the Fourier coefficients $AH_{k,l}$, followed by computation of $F(x,y,t)$ which in turn is transformed to Fourier space to obtain $AF_{k,l}$ using a fast Fourier transform (hence the nonlinear terms are evaluated in physical space and are then transformed to Fourier space).

[1] S. W. Joo, S. H. Davis, and S. G. Bankoff, J. Fluid Mech. **230**, 117 (1991).
[2] A. Oron and P. Rosenau, J. Phys. II **2**, 131 (1992).
[3] S. Kalliadasis, E. A. Demekhin, C. Ruyer-Quil, and M. G. Velarde, J. Fluid Mech. **492**, 303 (2003).
[4] P. M. J. Trevelyan and S. Kalliadasis, J. Eng. Math. **50**, 177 (2004).
[5] U. Thiele and E. Knoblock, Physica D **190**, 213 (2004).
[6] B. Scheid, C. Ruyer-Quil, U. Thiele, O. A. Kabov, J. C. Legros, and P. Colinet, J. Fluid Mech. **527**, 303 (2005).
[7] C. Ruyer-Quil, B. Scheid, S. Kalliadasis, M. G. Velarde, and R. Kh. Zeytounian, J. Fluid Mech. **538**, 199 (2005).
[8] B. Scheid, C. Ruyer-Quil, S. Kalliadasis, M. G. Velarde, and R. Kh. Zeytounian, J. Fluid Mech. **538**, 223 (2005).
[9] S. Kalliadasis, A. Kiyashko, and E. A. Demekhin, J. Fluid Mech. **475**, 377 (2003).
[10] B. Scheid, A. Oron, P. Colinet, U. Thiele, and J. C. Legros, Phys. Fluids **14**, 4130 (2002).
[11] J. M. Skotheim, U. Thiele, and B. Scheid, J. Fluid Mech. **475**, 1 (2003).
[12] P. M. J. Trevelyan, S. Kalliadasis, J. H. Merkin, and S. K. Scott, Phys. Fluids **14**, 2402 (2002).
[13] P. M. J. Trevelyan and S. Kalliadasis, Phys. Fluids **16**, 3191 (2004).
[14] P. M. J. Trevelyan and S. Kalliadasis, Phys. Fluids **16**, 3209 (2004).
[15] J. P. Burelbach, S. G. Bankoff, and S. H. Davis, J. Fluid Mech. **195**, 462 (1988).
[16] M. J. Tan, S. G. Bankoff, and S. H. Davis, Phys. Fluids A **2**, 313 (1990).
[17] J. P. Burelbach, S. G. Bankoff, and S. H. Davis, Phys. Fluids A **2**, 321 (1990).
[18] A. Oron, Phys. Fluids **12**, 1633 (2000).
[19] A. Oron, Phys. Rev. Lett. **85**, 2108 (2000).
[20] U. Thiele, M. G. Velarde, and K. Neuffer, Phys. Rev. Lett. **87**, 016104 (2001).
[21] M. Bestehorn, A. Potosky, and U. Thiele, Eur. Phys. J. B **33**, 457 (2003).
[22] U. Thiele, Eur. Phys. J. E **12**, 409 (2003).
[23] A. Sharma, Eur. Phys. J. E **12**, 397 (2003).
[24] A. Sharma and R. Verma, Langmuir **20**, 10337 (2004).
[25] S. Kalliadasis, C. Bielarz, and G. M. Homsy, Phys. Fluids **12**, 1889 (2000).
[26] S. Kalliadasis and G. M. Homsy, J. Fluid Mech. **448**, 387 (2001).
[27] A. Mazouchi and G. M. Homsy, Phys. Fluids **13**, 2751 (2001).
[28] C. M. Gramlich, S. Kalliadasis, G. M. Homsy, and C. Messer, Phys. Fluids **14**, 1841 (2002).
[29] C. Bielarz and S. Kalliadasis, Phys. Fluids **15**, 2512 (2003).
[30] J. M. Davis and S. M. Troian, Phys. Fluids **17**, 072103 (2005).

[31] A. Alexeev, T. Gambaryan-Roisman, and P. Stephan, Phys. Fluids **17**, 062106 (2005).
[32] Yu. O. Kabova, A. Alexeev, T. Gambaryan-Roisman, and P. Stephan, Phys. Fluids **18**, 012104 (2006).
[33] *Liquid Interfacial Systems—Oscillations and Instability*, edited by R. V. Birikh, V. A. Briskman, M. G. Velarde, and J. C. Legros (Marcel Dekker, New York, 2003).
[34] A. Oron, S. H. Davis, and S. Bankoff, Rev. Mod. Phys. **69**, 931 (1997).
[35] L. W. Schwartz, Langmuir **14**, 3440 (1998).
[36] L. W. Schwartz and R. R. Eley, J. Colloid Interface Sci. **202**, 173 (1998).
[37] L. W. Schwartz, R. V. Roy, R. R. Eley, and S. Petrash, J. Colloid Interface Sci. **234**, 363 (2001).
[38] R. C. Reid, J. M. Prausnitz, and T. K. Sherwood, *The Properties of Gases and Liquids* (McGraw-Hill, New York, 1977).
[39] *Handbook of Chemistry and Physics*, edited by D. R. Lide (CRC Press, Boca Raton, 1993).
[40] N. Fraysse and G. M. Homsy, Phys. Fluids **6**, 1491 (1994).
[41] O. Sandberg and B. Sundqvist, J. Appl. Phys. **53**, 8751 (1982).
[42] O. A. Kabov, I. V. Marchuk, and V. M. Chupin, Russ. J. Eng. Thermophys. **6**, 105 (1996).
[43] B. Scheid, A. Oron, P. Colinet, U. Thiele, and J. L. Legros, Phys. Fluids **14**, 4130 (2002).
[44] G. Teletzke, H. T. Davis, and L. E. Scriven, Chem. Eng. Commun. **55**, 41 (1987).
[45] N. Silvi and E. B. Dussan V., Phys. Fluids **28**, 5 (1985).
[46] E. Ramé, J. Colloid Interface Sci. **185**, 245 (1997).
[47] S. Saprykin, E. A. Demekhin, and S. Kalliadasis, Phys. Rev. Lett. **94**, 224101 (2005).
[48] S. Saprykin, E. A. Demekhin, and S. Kalliadasis, Phys. Fluids **17**, 117105 (2005).
[49] S. Saprykin, E. A. Demekhin, and S. Kalliadasis, Phys. Fluids **17**, 117106 (2005).
[50] R. Konnur, K. Kargupta, and A. Sharma, Phys. Rev. Lett. **84**, 931 (2000).
[51] K. Kargupta, R. Konnur, and A. Sharma, Langmuir **16**, 10243 (2000).
[52] K. Kargupta and A. Sharma, J. Colloid Interface Sci. **245**, 99 (2002).
[53] A. Sharma, Eur. Phys. J. E **12**, 397 (2003).
[54] U. Thiele, L. Brush, M. Bestehorn, and M. Bár, Eur. Phys. J. E **11**, 255 (2003).
[55] D. E. Kataoka and S. M. Troian, Nature (London) **402**, 794 (1999).
[56] L. Kondic and J. Diez, Phys. Fluids **16**, 3341 (2004).
[57] L. E. Stillwagon and R. G. Larson, J. Appl. Phys. **63**, 5251 (1988).
[58] L. E. Stillwagon and R. G. Larson, Phys. Fluids A **2**, 1937 (1990).
[59] L. M. Peurrung and D. B. Graves, IEEE Trans. Semicond. Manuf. **6**, 72 (1993).